Macromolecules

Article

pubs.acs.org/Macromolecules

Heterogeneous Lamellar Structures Near the Polymer/Substrate Interface

M. Asada,[†,‡] N. Jiang,[†] L. Sendogdular,[†] P. Gin,[†] Y. Wang,[†] M. K. Endoh,[†,*] T. Koga,[†,*] M. Fukuto,[§] D. Schultz,[⊥] M. Lee,[⊥] X. Li,[∥] J. Wang,[∥] M. Kikuchi,[○] and A. Takahara[○,#,*]

[†]Department of Materials Science and Engineering, Stony Brook University, Stony Brook, New York 11794-2275, United States

[‡]Kurashiki Research Center, Kuraray Co., Ltd., 2045-1 Sakazu, Kurashiki, Okayama 710-0801, Japan

[§]Condensed Matter Physics and Materials Science Department, Brookhaven National Laboratory, Upton, New York 11973, United States

[⊥]CARS, University of Chicago, Chicago, Illinois 60637, United States

[∥]Advanced Photon Source, Argonne National Laboratory, Argonne, Illinois 60439, United States

[○]Japan Science Technology Agency, ERATO, Takahara Soft Interfaces, CE80, Kyushu University, 744 Motooka, Nishi-ku, Fukuoka 819-0395, Japan

[#]Graduate School of Engineering, Kyushu University, 744 Motooka, Nishi-ku, Fukuoka 819-0395, Japan

ABSTRACT: We report the structural heterogeneity of recrystallized linear low-density polyethylene (LLDPE) films (25, 50, and 100 nm in thickness) in the direction normal to the surface, based on *in situ* grazing incidence small-angle X-ray scattering (GISAXS) and X-ray diffraction (GID) measurements. The GID results have clarified the presence of the edge-on lamellae at the surfaces and in the interior of the LLDPE films prepared on Si substrates as thin as 25 nm in thickness. However, the degree of the crystallinity for the 25 nm thick film was almost half of those for the 50 and 100 nm thick films, while the melting temperature (T_m) for all the films remained unchanged relative to the bulk (T_m = 117 °C). Moreover, the GISAXS results for the 25 nm thick film indicate the structural heterogeneity in the direction normal to the surface: (i) At the polymer/air interface, the presence of the disordered edge-on lamellae which lack well-defined long periods even at $T \ll T_m$; (ii) At the polymer/substrate interface, the persistence of a substrate-bound edge-on lamellar layer even at $T \gg T_m$; (iii) In between the two interfacial layers, the existence of the well-ordered edge-on lamellae with the long periods. These heterogeneous structures can be explained as a consequence of the nucleation initiated at the topmost surface of the substrate-bound lamellar layer.

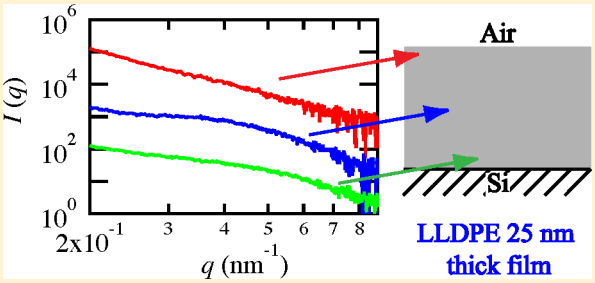

I. INTRODUCTION

Polymer thin films on solid substrates have been explored in a variety of industrial fields owing to their advantages including inexpensiveness, lightweight, flexibility, and facile fabrication of desired molecular architectures.[1] At the same time, the unusual properties of polymer thin films due to the effects of confinement, such as viscoelastic property,[2,3] glass transition temperature (T_g),[4,5] interdiffusion,[6,7] and physical aging,[8] have been acknowledged from an academic point of view. There is growing evidence that the interplay between the polymer/air and polymer/substrate interfaces is crucial to understand the mechanism of the confinement effects.[8,9] At the polymer/air interface, there exists a surface mobile layer,[10−12] which enhances the chain dynamics. Previous studies showed that the rate of crystallization, crystal orientation, and density of nucleation sites for polymer thin films are quite different from the bulk.[13−19] In addition, grazing incidence X-ray diffraction experiments clarified that the lattice constants, crystallinity, the degree of paracrystalline lattice distortion,[20] and the crystallization kinetics[21] at the surface are quite different from those of the rest of the film. On the other hand, the substrate interface is known to reduce the dynamics because of an immobile polymer adsorbed layer[22−27] including semicrystalline polymers.[25,26] However, little is known about the effect of the substrate interface on local structures or properties within semicrystalline polymer thin films.

In this paper, we utilize a combination of *in situ* grazing incidence small-angle X-ray scattering (GISAXS) and X-ray diffraction (GID) with two different incident angles of X-ray beams to provide a better understanding of the local structures of recrystallized polymer thin films. Spin-cast linear low-density polyethylene (LLDPE) thin films (25, 50, and 100 nm in thickness) prepared on cleaned hydrogen-passivated silicon (H−Si) substrates were used as the model system, because the

Received: May 17, 2012
Revised: July 20, 2012
Published: August 31, 2012

crystalline structures and melting behavior in the bulk LLDPE have been well characterized. Furthermore, the combined use of transmission small-angle X-ray scattering (SAXS), transmission wide-angle X-ray scattering (WAXS), and differential scanning calorimetry (DSC) experiments for the bulk LLDPE resin enabled us to highlight the deviations of the recrystallized structures of the ultrathin films and its melting behavior from the bulk. As a result, we found the presence of heterogeneous architectures within the 25 nm thick film in the direction normal to the surface: (i) At the polymer/air interface, there exist the disordered edge-on lamellae which lack a well-defined interlamellar spacing, so-called "long period", even at temperatures far below the bulk melting temperature (T_m). (ii) At the polymer/substrate interface, the polymer chains adsorb onto the substrate and the substrate-bound edge-on lamellar structures remain even at $T \gg T_m$. (iii) In between the two interfacial layers, the polymer chains form the well-ordered edge-on lamellae and the melting behavior is governed by the sequential melting as seen in the bulk.[28−30] According to the previous results where polymer chains were quenched from the melt to a low crystallization temperature,[19] the nucleation was found to be triggered at the polymer/air interface due to the surface mobile layer. However, it is not conclusive whether the surface mobile layer is present within a few tens of nanometer thick supported films.[9] Therefore, we postulate that the recrystallization is initiated from the substrate-bound lamellar layer as seeds, independently of the primary nucleation at the polymer/air interface. Furthermore, we reveal that this substrate effect associated with the substrate-bound lamellar layer is limited to the region within 50 nm from the substrate interface for the present system.

II. EXPERIMENTAL SECTION

II.1. Sample Preparation. LLDPE (molecular weight (M_w) = 50 000, polydispersity = 2, T_m = 117 °C) was kindly provided by ExxonMobil Corporation. Si substrates were cleaned by immersion in a hot piranha solution (i.e., a mixture of H_2SO_4 and H_2O_2 [Caution! The piranha solution is highly *corrosive* upon contact with the skin or eyes and is an explosion hazard when mixed with organic chemicals/materials. Extreme care should be taken when handing it.] for 15 min, subsequently rinsed with purified water thoroughly, and followed by submersion in an aqueous solution of hydrogen fluoride to remove native oxide. Three different thin films with average thicknesses of 25, 50, and 100 nm were prepared by spin coating PE/toluene solutions onto hydrogen-passivated Si substrates above 100 °C. The details of the film preparation has been described elsewhere.[17] All samples were dried under vacuum at 150 °C for 24 h to erase the memory of the sample preparation and then rapidly quenched to room temperature within 1 min in order to recrystallize the films. The surface tension of the LLDPE is 30 mJ/m^2.[31] The interfacial energy (γ) between the polymer and the substrate is then estimated to be $\gamma_{PE/Si}$ = 6.2 mJ/m^2 based on the Owens−Wendt−Kaelble equation[32] with the dispersion part (48.71 mJ/m^2) and polar part (3.98 mJ/m^2) of the surface tension of Si.[18] Compared with $\gamma_{PS/Si}$ = 1.4 mJ/m^2 for the polystyrene/Si system or $\gamma_{PB/Si}$ = 4.0 mJ/m^2 for the polybutadiene/Si system, the LLDPE film prepared on a Si substrate is categorized as a weakly attractive interacting system.

II.2. Ellipsometry. The average thickness of the recrystallized LLDPE films was measured by AutoEL-II ellipsometry (Rudolf Research) equipped with a He−Ne laser (632 nm) by setting the index of refraction for LLDPE as 1.53.

II.3. Scanning Force Microscope (SFM) Measurements. *In situ* surface crystalline morphologies of the LLDPE thin films were observed by a scanning force microscope (SFM) (Seiko Instruments Inc., E-sweep). Dynamic force microscopic mode measurements were carried out under vacuum as to avoid the surface oxidation and a capillary force effect induced by surface-adsorbed water. As will be discussed later, the surface morphology of the adsorbed (residual) layer after an intensive washing process with toluene (a good solvent for LLDPE) was measured by a contact mode SFM (Dimension 3100, Digital Instruments).

II.4. DSC Measurements. Melting behavior of the bulk LLDPE was characterized by DSC (Perkin-Elmer DSC 7) in a nitrogen atmosphere. Figure 1 shows the DSC curve obtained at the heating rate of 5 °C/min. From the figure, we can see that the melting starts at around 90 °C and ends at 117 °C. We also confirmed that the DSC curves obtained with different heating rates remain unchanged. The enthalpy of melting (ΔH_m) was calculated to be 80 J/g from the area of the DSC peak between 90 and 117 °C after the baseline (indicated as the dotted line) subtraction. The degree of crystallinity (ϕ_b) in the bulk was then estimated to be 0.27 by using the following equation:

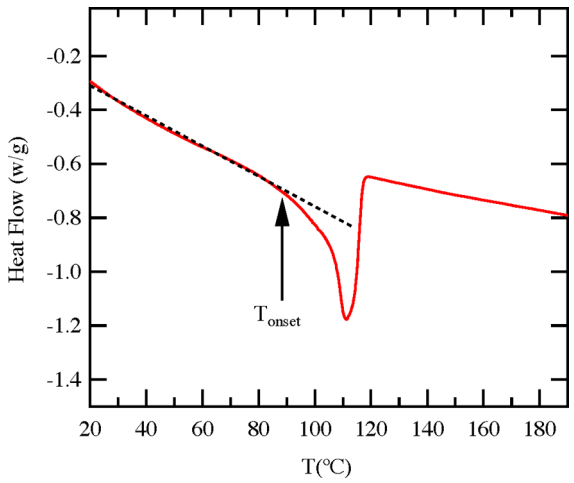

Figure 1. Heat flowchart of the LLDPE resin at a heating rate of 5 °C/min.

$$\phi_b = \frac{\Delta H_m}{\Delta H_{100}} \quad (1)$$

Here ΔH_{100} is the value of heat fusion for the 100% crystalline polymer. For this study, $\Delta H_{100} = 293 J/g$ was used.[33] We confirmed that the crystallinity is in good agreement with the one determined by WAXS experiments.

II.5. GISAXS Measurements. *In situ* GISAXS study was conducted at the sector 8-ID beamline, Advanced Photon Source (APS, Argonne). The details have been described elsewhere.[34] The scattering from each sample was collected by a 2D MAR-CCD camera for an accumulation time of 10 s. Two-dimensional (2d) GISAXS profiles were obtained with successive heating and cooling temperature runs from room temperature (20 °C) to 150 °C after 30 min stabilization at each temperature. GISAXS measurements are advantageous for quantitatively characterizing edge-on lamellae oriented in the direction perpendicular to the substrate surface (as schematically shown in Figure 4a), while flat-on lamellae where the lamellar layers run parallel to the surface cannot be detected with this scattering geometry. In order to see the differences in the crystalline structures between the topmost surface and the rest of the film, the two different incident angles (α) were utilized: (i) $\alpha = 0.13°$, which is just below the critical angle (α_c) of the total external reflection for LLDPE (α_c = 0.16° with an X-ray energy of 7.4 keV used in this study) such that the electric field intensity decays exponentially into the film and thereby scattering intensity is dominated by the surface area of about 9 nm depth; (ii) $\alpha = 0.18°$, above α_c, where the X-ray penetration depth (~3 μm) exceeds the film thickness such that we can obtain information on average structures over the entire film. We denote the first experimental configuration as the "*surface-mode*" and the second one as the "*film-mode*" hereafter. Note that, as shown in Figure 2, the

dx.doi.org/10.1021/ma301000z | *Macromolecules* 2012, 45, 7098−7106

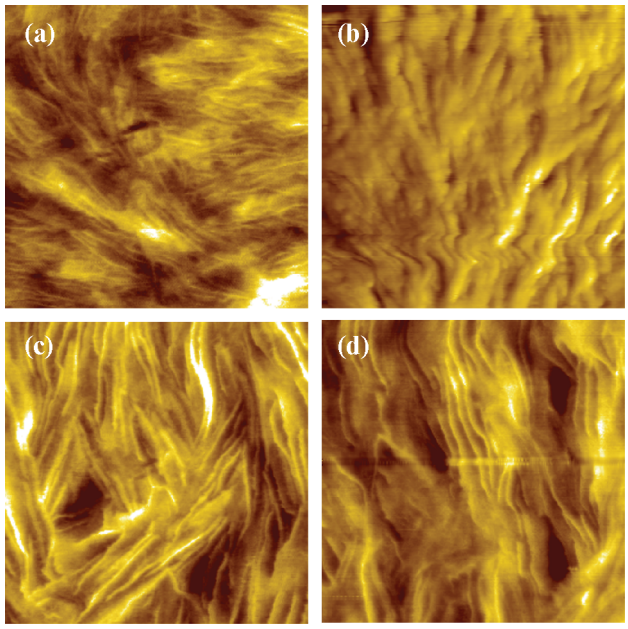

Figure 2. Surface topographic crystalline morphology obtained by SFM measurements: (a) the 100 nm thick film at room temperature (T = 25 °C); (b) the 100 nm thick film at T = 80 °C; (c) the 25 nm thick film at room temperature; (d) the 25 nm thick film at T = 40 °C, respectively. The scan sizes and height scales for all the images are 1 μm × 1 μm and 0–20 nm, respectively.

surfaces of the LLDPE films at low temperatures may not be a "mirror" (the root-mean-square roughness values are approximately 4 nm for the 50 and 100 nm thick films and 2 nm for the 25 nm thick film, respectively) so that the X-ray beams may penetrate into the film interior more than 9 nm in depth. Nevertheless, as will be discussed later, the GISAXS profiles for the 25 nm thick film are quite different between the surface-mode and the film-mode. In addition, as the temperature increases, the degree of the crystallinity for all the films decreases and the resultant surfaces become more flattened. For these reasons, we conclude that the two modes are still able to differentiate the structures at the topmost surface and over the entire film. To prevent possible errors associated with the rough surface, analysis for the GISAXS and GID data was performed only at high temperatures (i.e., $T \geq 60$ °C).

II.6. GID Measurements. *In situ* GID measurements with the aforementioned two modes were performed at the beamline x22B at the National Synchrotron Light Source (NSLS, Upton) for acquiring 2d images with a CCD camera (Princeton Instruments). An X-ray energy of 8.17 keV was used. High temperature GID experiments, up to 100 °C, were performed by using a custom-built vacuum furnace with Be windows. In addition, one-dimensional (1d) profiles near the (110) Bragg reflections were measured as a function of temperature (up to 140 °C) by using a scintillation counter (Oxford), scanning in the direction parallel to the sample surface (i.e., an in-plane configuration) at the sector 15-B beamline (APS).

II.7. Transmission SAXS and WAXS Measurements. Transmission WAXS and SAXS experiments for the bulk resin were performed at the beamline x27C at the NSLS. A MAR CCD detector (Rayonix, L.L.C.) was used to obtain 2d images. The details of the experimental setup have been described elsewhere.[35] Since both SAXS and WAXS scattering patterns were isotropic, the scattering profiles were integrated over the azimuthal angle after corrections for air scattering and incident beam intensity fluctuations and converted into 1d profiles to further analyze the data. The degree of crystallinity (X_c) in the irradiated area of the LLDPE films was then estimated from the 1d WAXS profiles as follows:

$$X_c = \frac{\sum I_c(q)}{\sum I_c(q) + \sum I_a(q)} \quad (2)$$

Here I_c and I_a are intensities from the crystalline and amorphous components at the scattering vector q (= $4\pi \sin\theta/\lambda$, θ being half the scattering angle and λ the wavelength of X-rays) respectively. The values of these peaks were determined by the best-fits of the experimental profiles with the predicted profiles constructed by a weighted average of Lorentzian and Gaussian functions for the broad amorphous and sharp crystalline components, respectively.

III. RESULTS

III.1. SFM Experiments. Before the X-ray scattering experiments, we utilized SFM to characterize the surface structures. Figure 2a shows a SFM height image of the 100 nm thick film at room temperature (T = 25 °C) where the bright and dark areas correspond to higher and lower heights at the surface, respectively. The sheaf-like morphology has been assigned to a crystalline lamellar structure oriented edge-on with respect to the film surface.[17] At around T = 80 °C, the sheaf-like aggregates become more flattened (Figure 2b) and we could not capture the phase images at T > 90 °C due to surface softening, which occurs near the bulk melting temperature (see Figure 1). The surface morphologies of the 50 nm thick film (data not shown) are quite similar to those of the 100 nm thick film. As shown in Figure 2c, similar sheaf-like aggregates can also be seen in the 25 nm thick film at room temperature; however, the stacked lamellar structures are less dense than those in the 50 and 100 nm thick films. In addition, the surface softening of the 25 nm thick film occurred at substantially lower temperatures, around 40 °C (Figure 2d), and this prevented the phase imaging at higher temperatures. These SFM results suggest a significant decrease in the crystallinity and a change in the lamellar structures of the 25 nm thick film compared to those of the thicker films. Below, we show that the combined use of GISAXS and GID techniques enabled us to quantitatively characterize the *in situ* structures and melting behavior at the surface and in the entire film independently.

III.2. GID Experiments. Figure 3 shows representative GID results for the 25 nm thick films at room temperature. We can

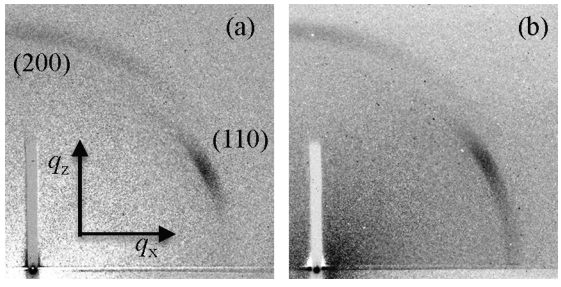

Figure 3. Representative two-dimensional GID images for the 25 nm thick film at room temperature: (a) surface-mode; (b) film-mode. The specular reflection is shielded by a beam stop seen as the rectangular shape.

see that the 2d GID patterns are nearly identical between the surface-mode (Figure 3a) and film-mode (Figure 3b). We also confirmed that the same is true for the 50 and 100 nm thick films. We can index the two Bragg reflections at q = 15.1 nm^{-1} and 16.3 nm^{-1} as (110) and (200), respectively, based on the known LLDPE orthorhombic crystal structure with the unit cell parameters: a = 7.4 Å, b = 4.93 Å, c = 2.53 Å.[36] In addition,

(200) is located along the surface normal, while the (110) reflection is found at the off-axis position. This indicates that the LLDPE crystal structures are preferentially oriented with respect to the substrate. In order to determine the orientation (either edge-on or flat-on) of the crystal structures, we simulated the reflection patterns by assuming that the polymer chain axis is identical to the crystallographic *a*, *b* or *c*-axis, as schematically shown in Figure 4a. The details of the simulations

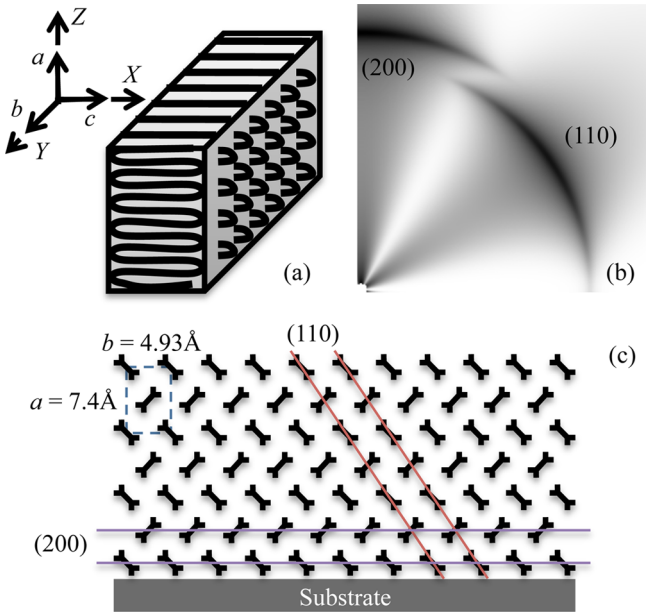

Figure 4. (a) Crystal geometry (edge-on) in the film plane used for simulated diffraction pattern, (b) the resultant simulated diffraction pattern, and (c) the schematic crystal model viewed along the chain axis (the *c*-axis). Each symbol corresponds to the monomeric unit.

have been described elsewhere.[37] Comparisons between simulated patterns (Figure 4b) and the observed GID patterns led to the conclusion that the LLDPE chains form the edge-on lamellae with its crystallographic *c*-axis pointing along the direction parallel to the surface, as schematically shown in Figure 4c. This is consistent with the SFM results (Figure 2) where the surfaces of the films are mainly covered with the edge-on lamellar structures.

Figure 5 shows the temperature dependences of the intensity (the film-mode) integrated near the (110) reflection peak position and normalized by the film thickness for the 25 and 50 nm thick films. The results for the 100 nm thick films are nearly identical to that for the 50 nm thick film. From the figure we can see that the thickness-normalized intensity for the 25 nm film is about half of the 50 nm thick film regardless of temperature. It is also important to point out that the intensities for the 25 and 50 nm thick films suddenly drop off at around $T = 90$ °C and completely disappeared at the bulk T_m (=117 °C) obtained from the DSC and WAXS experiments. Figure 5 also shows that the temperature dependence of the bulk crystallinity determined by WAXS (indicated by the crosses) has the same trend as the intensity changes for the thick films. These observations demonstrate that the integrated intensity represent a direct measure of the crystallinity within the thin films. Thus, the GID results provide the evidence that the onset of melting occurs at around 90 °C for the thin films and that the crystallinity of the 25 nm thick film is considerably

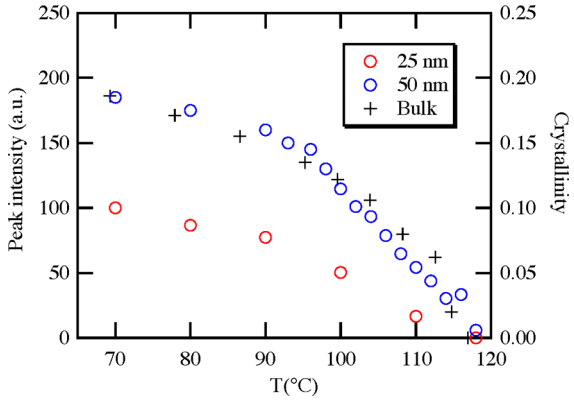

Figure 5. Integrated intensity near the (100) Bragg reflection peak as a function of temperature for the 25 nm (red) and 50 nm (blue) thick films obtained by the GID results. The crystallinity of the bulk determined by WAXS is indicated as the black crosses.

suppressed relative to the 50 and 100 nm thick films. A series of the GID experiments also led to the conclusion that the melting temperatures at the topmost surface and of the entire film, as measured by the disappearance of the (110) and (200) peaks, remain essentially the same as the bulk T_m regardless of the film thicknesses. It should be noted that, as will be discussed later, there exists a very thin substrate-bound lamellar layer even at $T \gg T_m$. We presume that the degree of crystallinity in the substrate-bound lamellar layer is very low so that the present GID experiments in the film mode may not be sensitive enough to identify the layer.

III.3. GISAXS Results. Figure 6 shows the temperature dependences of the GISAXS profiles for the 100 nm thick film in the surface-mode (Figure 6a) and the film-mode (Figure 6b) during the heating process. The 2d profiles were used to extract the 1d profiles of the intensity along the q_{xy}-direction at around $q_z = 0.1$ nm^{-1}. From these figures we can see the broad scattering maximum at around the in-plane scattering vector ($q_{||}$) of 0.4 nm^{-1} at $T < T_m$ in both the surface-mode and film-mode. The peak is attributed to the lamellar long period (L_p) of the edge-on lamellae. As the temperature increases, the peak position shifts to the lower *q*-region at $T \leq T_m$. At the same time, the weak broad shoulder (indicated by the arrow) is observed in the film-mode even at $T > T_m$, whereas the broad peak in the surface-mode disappears at the same temperature range. This broad shoulder implies the persistence of an edge-on lamellar layer within the film even at $T > T_m$. It should be noted that the GISAXS profiles in the film-mode and surface-mode at 120 °C $< T \leq$ 150 °C are almost identical to the ones at $T = 120$ °C. Further discussion about the substrate-bound lamellar layer will be presented later.

In order to calculate the long periods, the GISAXS data was analyzed in terms of a 1d model of stacked lamellar crystals separated by amorphous layers.[38] The normalized 1d correlation function can be obtained by the following equation:

$$\gamma(r) = \frac{\int_0^\infty I(s)s^2 \cos(2\pi rs)\, ds}{\int_0^\infty I(s)s^2\, ds} \quad (3)$$

where *s* corresponds to the magnitude of $2\pi/q_{||}$ and *r* represents the distance in a real space. Before calculations of the correlation functions, several corrections including smoothing using spline functions to reduce the effect of noise and extrapolations to both low and high *s* values to extend the

dx.doi.org/10.1021/ma301000z | Macromolecules 2012, 45, 7098–7106

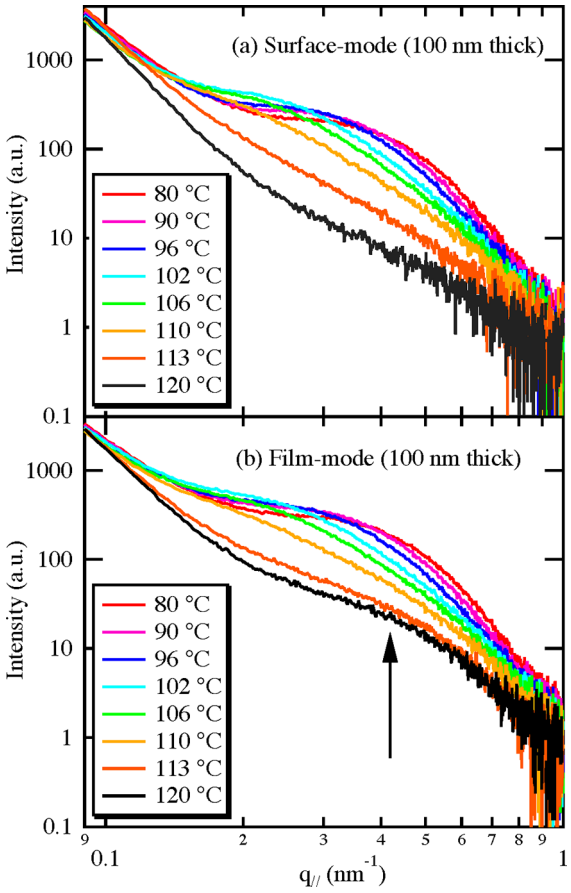

Figure 6. GISAXS profiles for the 100 nm thick films with elevating temperature up to 120 °C. (a) surface-mode; (b) film-mode. The arrow indicates the presence of the weak broad shoulder even at $T > T_m$.

limited experimental s values were made.[39] Extrapolation to $s \rightarrow 0$ can be performed by the Debye−Bueche model:[40]

$$I(s) = \frac{C}{(1 + 4\pi^2\xi^2 s^2)^2} \quad (4)$$

where C is a constant and ξ is an inhomogeneity length. On the other hand, extensions of intensity to large s values could be achieved according to the Porod−Ruland model[41]

$$\lim_{s\rightarrow 0} I(s) = P\frac{e^{-4\pi^2\sigma^2 s^2}}{s^4} \quad (5)$$

where P is the Porod constant and σ is the interfacial width between the crystalline and amorphous regions in lamellar stacks. Figure 7 shows the temperature dependence of the long periods $L_p(T)$ for the 100 nm thick film in the film-mode obtained by the position of the first maximum of $\gamma(r)$. The temperature dependence of the long period in the surface-mode for the 100 nm thick film (data not shown) is exactly identical to that in the film-mode at $T \leq T_m$. From the figure we can see a slight increase in $L_p(T)$ up to $T \cong 80$ °C from the original value (L_p^0) of 11.5 nm at room temperature ($T = 25$ °C). A rapid increase in L_p is then observed above $T = 90$ °C, which corresponds to the onset of the melting temperature. As shown in the inset, the values of $L_P(T)/L_p^0$ for the 100 nm thick film (indicated by triangles) are in good agreement with those for the bulk (indicated by crosses) obtained by SAXS. This strong increase in the long periods at $T \geq 90$ °C has been

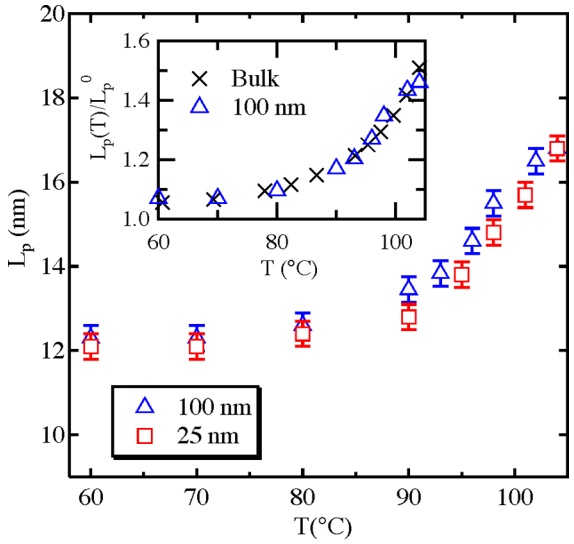

Figure 7. Long periods (L_p) of the lamellar structure vs temperature for the 25 and 100 nm thick films determined in the film mode. The temperature dependence of L_p for the bulk resin is also plotted in the inset of the figure.

reported previously in bulk LLDPE and high density PE[39,42,43] and can be explained by the sequential melting (i.e., the melting of some randomly placed crystals within stacks, resulting in an increase in the average amorphous thickness[28−30]). Since the temperature dependence of L_p for the 50 nm thick film is consistent with that for the 100 nm thick film, we conclude that the melting processes for the 50 and 100 nm thick films are governed by the sequential melting as for the bulk.

We now turn to the melting process for the 25 nm thick film where the significant decrease in the degree of the crystallinity is identified by GID. The GISAXS profiles in the surface-mode and film-mode are shown in Figure 8. The GISAXS profiles in the film-mode clearly show the broad scattering maximum corresponding to the long period of the edge-on lamellae at around $q_\parallel = 0.4$ nm^{-1} (Figure 8b). In addition, as indicated in Figure 6b for the 100 nm thick films, the broad shoulder persists even at $T \geq T_m$, demonstrating the presence of the substrate-bound lamellar layer in the 25 nm thick film as well. In contrast, as shown in Figure 8a, there is no scattering peak in the surface-mode for the 25 nm thick film. In conjunction with the GID data and SFM images, the GISAXS data is consistent with the absence of the well-defined long periods at the surface of the 25 nm thick film. In order to provide further insight into the disordered edge-on lamellar structures at the surface, we used the Debye-Bueche (DB) analysis[40] (eq 4) with the assumption of a random two-phase system composed of a crystal region and amorphous region in the lamellar stack. Figure 9a shows representative $I(q_\parallel)^{-0.5}$ vs $q_\parallel^2$ plots at $T = 90$ and 104 °C for the 25 nm thick (surface-mode) film. From the slope (c_1) and intercept (c_2) at $q_\parallel = 0$ in these plots, the correlation distances $(\xi = (c_1/c_2)^{1/2})$ were calculated. Figure 9b plots the temperature dependence of ξ obtained from the fits with the $q_\parallel$-range of $0.27 < q_\parallel < 0.42$ nm^{-1}. From the figure we can see the similar trend of ξ to the long periods: at around $T = 90$ °C, ξ starts to increase on raising temperature toward T_m. Judging from this behavior, we assume that ξ corresponds to the thickness of the amorphous region in the lamellar stack, even though the magnitude is smaller than that formed in the bulk film (10−15 nm in thickness estimated from the product

dx.doi.org/10.1021/ma301000z | Macromolecules 2012, 45, 7098−7106

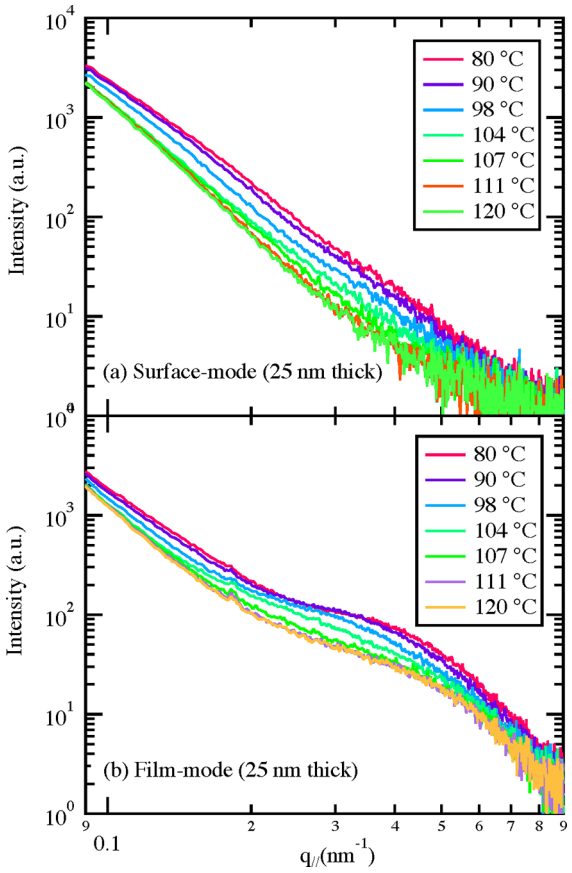

Figure 8. GISAXS profiles for the 25 nm thick film with elevating temperature: (a) surface-mode; (b) film-mode.

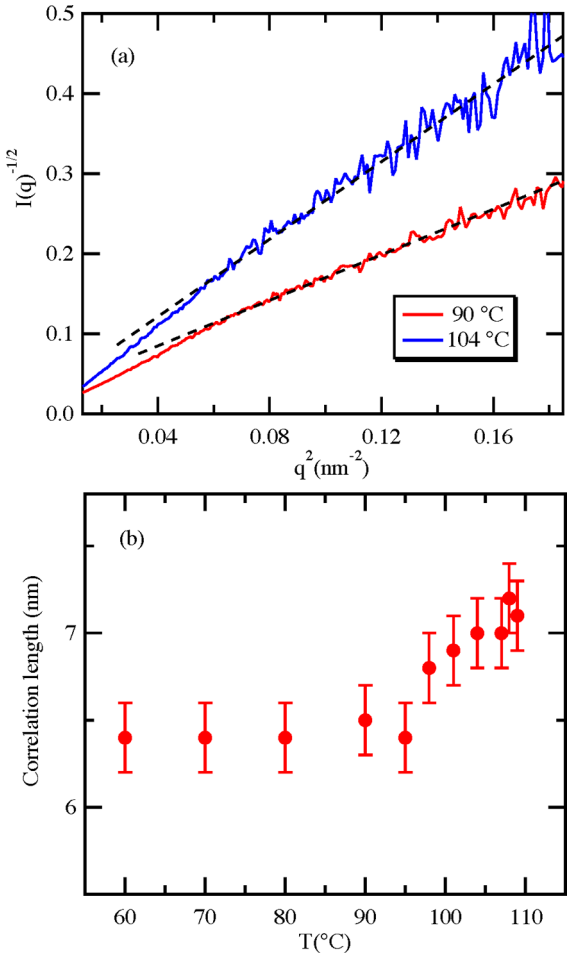

Figure 9. (a) Representative DB plots for the 25 nm thick film (surface-mode) at T = 90 and 107 °C. (b) Temperature dependence of the correlation distances existing in the lamellar stack.

of L_p and $(1 - X_c)$). We also stress the deviation from the linear relationship of $I(q_{\|})^{-0.5}$ vs $q_{\|}^2$ at the lower $q_{\|}$ range ($q_{\|}^2 <$ 0.06 nm^{-2}), indicative of another larger heterogeneous structure with $\xi \sim 25$ nm based on the DB analysis. Since T_m at the surface of the 25 nm thick film remains unchanged relative to the bulk T_m, the thickness of the crystalline region in the lamellar stack, which is related to T_m (the Thomson-Gibbs equation[44,45]), should be equivalent to that for the bulk film. Therefore, we assume that this larger ξ value also corresponds to the thickness of the amorphous region in the lamellar stack, indicating the presence of the in-plane heterogeneities in L_p at the surface of the 25 nm thick film.

IV. DISCUSSION

The key question is why the surface order including the crystallinity, the lamellar stacking, and the long periods are significantly reduced/or distorted when the thickness of the LLDPE films is reduced to 25 nm. Below we address the question by clarifying the interior architecture of the 25 nm thick film in more detail.

First, we focus on the buried structure near the substrate interface. For this purpose, the LLDPE films used for GISAXS experiments were washed at least 10 times (each washing was for approximately 30 min) in baths of fresh toluene at T = 90 °C. After the washing process, we annealed the remaining layers at T = 150 °C for 2 h to remove any excess solvent trapped in the layers and measured the thickness by using ellipsometry. As a result, we found the presence of a residual (adsorbed) layer of approximately 8 nm in thickness regardless of the original film thickness. Figure 10 shows the surface height image of the

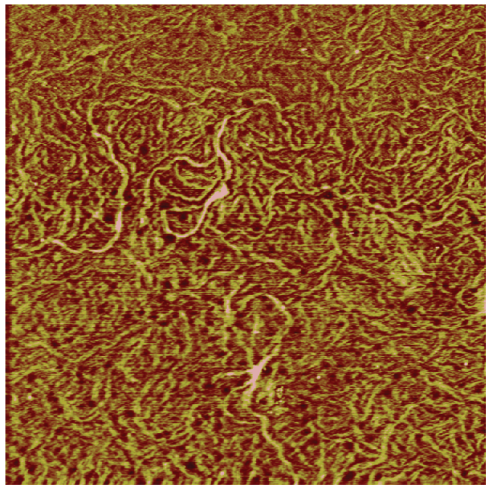

Figure 10. SFM height image of the residual LLDPE film at room temperature. The image size and height scale are 5 μm × 5 μm and 0–20 nm, respectively.

residual LLDPE layer obtained by using SFM. From the figure, we can see the string-like structures which resemble typical edge-on lamellar structures formed in ultrathin polymer films.[19] Hence, we conclude that the adsorbed layer, which was not dissolved during the intensive washing process, is associated

dx.doi.org/10.1021/ma301000z | Macromolecules 2012, 45, 7098–7106

with the substrate-bound lamellar layer observed in the GISAXS profiles. However, we found that GISAXS measurements on the adsorbed layer (performed at the beamline BL03XU, SPring-8, Japan; the detail of the beamline has been described elsewhere[46]) do not show any broad shoulder (data not shown). This suggests that the long-range order in the residual film is destroyed during the solvent washing, preventing quantitative characterization of the substrate-bound lamellar layer formed in the original spin-cast thin films. Hence, no further measurements on the substrate-bound lamellar layer were performed in the present study.

Although this preferential edge-on orientation of the lamellae at the Si substrate can be explained by the concept of minimization of the free energy during the primary nucleation step,[17,47] its formation mechanism has not been clarified. We propose that the substrate-bound lamellae are formed during the spin-coating of the hot polymer/toluene solutions onto heated Si substrates at around T = 150 °C. This high temperature spin-coating was necessary to prevent the films from immediate crystallization on the substrates, which often causes dewetting.[17] The spin-cast films were then rapidly quenched to room temperature, inducing crystallization of the polymer chains within the entire film. Although we preannealed the films at T = 150 °C for 24 h to erase the memory of the sample preparation before recrystallization, the GISAXS results prove that this is not sufficient to completely melt the lamellae formed near the substrate interface. Instead, the long high temperature preannealing may accelerate the growth of the adsorbed layer[23] and induce reorganization of the chain conformations deformed during the spin-coating process.[48] Since the structural relaxation of the polymer chains adsorbed onto solid substrates is typically very slow,[49,50] the structures/properties of the adsorbed layer are considered as "metastable" states with extremely long lifetime.[23] Hence, we suppose that the substrate-bound lamellar structure is also attributed to the metastable conformations associated with the reduced chain mobility.

We further explore the interior architecture of the 25 nm thick film. Assuming that the scattering profile from the substrate-bound lamellar layer remains unchanged with changing temperature during the GISAXS experiments, we subtracted the scattering profile at T = 150 °C as additional background from the observed GISAXS profiles in the film-mode. Figure 11 shows the film-mode GISAXS profiles after this subtraction. From the figure it is clear that the shoulder-like scattering feature, which originates from the interior region between the two interfacial regions, shifts to the lower q-region upon approaching T_m. Interestingly, the long periods at $T \geq 60$ °C obtained by using eq 3 are in good agreement with those of the 50 and 100 nm thick, as plotted together in Figure 7. This implies that the 25 nm thick film's interior region still shows the bulk-like (sequential) melting behavior, in sharp contrast to the behavior of the substrate-bound lamellar layer. Hence, the GISAXS results elucidate that the structures of the 25 nm thick film are quite heterogeneous in the direction normal to the surface.

These results provide insight into the formation process of the heterogeneous structures within the 25 nm thick film. According to the previous results where polymer chains were quenched from the melt to a low crystallization temperature,[19] the nucleation was found to be triggered at the polymer/air interface due to the surface mobile layer. However, it is not conclusive yet whether the surface mobile layer is present

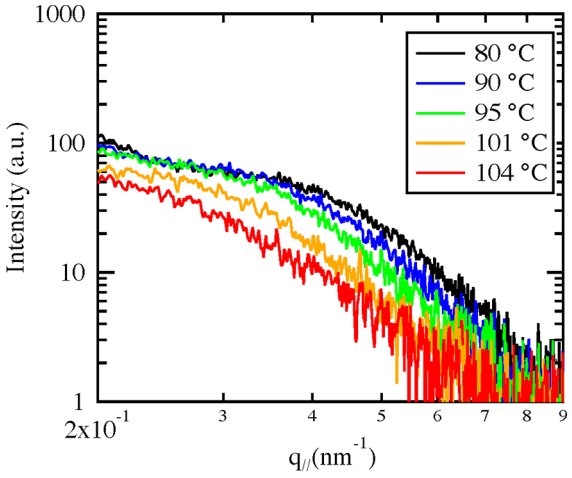

Figure 11. GISAXS profiles in the film-mode for the 25 nm thick film after subtraction of the scattering intensity at T = 150 °C.

within a few tens of nanometer thick films prepared on solid substrates.[9] Instead, the present results indicate that the polymer/substrate interface plays a vital role in inducing the heterogeneous structures. It is known that there exists the so-called "reduced mobility interface (RMI) layer"[51,52] in which the polymer chains are entangled with the adsorbed layer and act as a "transition zone" ensuring continuity in the mobility profile from the substrate to the bulk through chain entanglements.[35] Napolitano et al. reported that the RMI layer of poly(ethylene terephthalate) thin films prepared on aluminum substrates is about 20 nm in thickness.[25] Noting that the extent of the RMI layer should depend on the strength of the substrate interaction and the flexibility of polymer chains, it is reasonable to suppose that the part or whole of the interior region of the 25 nm thick LLDPE film corresponds to the transition zone. We therefore postulate that the recrystallization is initiated from the substrate-bound lamellar layer as seeds, independently of the primary nucleation at the polymer/air interface. The polymer chains in the transition zone would then form the edge-on lamellae with the same orientation as for the substrate-bound lamellar layer in order to maximize the contacts, thereby stabilizing the interface.[53] Consequently, the surface disordering is attributed to the substrate effect induced by the substrate-bound lamellar layer. In fact, we found that the recrystallized structures and melting behavior at the surfaces of the 50 and 100 nm thick films recover to bulk (thick film)-like due to the effect of the surface mobile layer,[19] while the substrate-bound lamellar layer is found to be formed regardless of the film thickness. Hence, we conclude that this substrate effect is limited to the region within 50 nm from the substrate interface. We are currently investigating to find the critical thickness, above which the bulk behavior is recovered, for different polymer/substrate systems, in order to elucidate the correlation between the critical thickness and the strength of the interactions, the flexibility of the polymer chains, or the size of polymer chains. We are also studying a reorganization process of polymer chains in the crystalline state that occurs even after growth of crystalline structures[54,55] so as to answer the question of why such constrained polymer chains in the transition zone form the well-ordered lamellae during the rapid recrystallization process.

The present results differ from the previous reports[17,18] which showed the presence of the flat-on lamellae at the surface

dx.doi.org/10.1021/ma301000z | Macromolecules 2012, 45, 7098−7106

of the 25 nm LLDPE thick film with the melting temperature of approximately 30 °C lower than the bulk T_m. We believe that these apparent inconsistencies are mainly due to the difference in the recrystallization process. It was reported that when the thickness of semicrystalline polymer thin films is less than 30 nm, the formation of edge-on lamellae is preferred at lower crystallization temperature close to T_g of the polymer, while flat-on lamellae become dominant at higher crystallization temperatures closer to bulk T_m.[47] In the present study, we quenched the LLDPE films from 150 °C to room temperature within 1 min, while Wang and co-workers crystallized their LLDPE thin films by slowly quenching from 140 °C to room temperature over a period of 12 h[17] such that their crystallization temperature should be closer to the bulk T_m. In addition, we realized that the annealing times at the high temperature before recrystallization, which are crucial for the formation of the adsorbed layer at the substrate interface,[23] are also quite different: 24 h for the present case and 0.5 h for the Wang and co-worker's experiments. As described above, since the adsorption process is typically very slow (several hours) for long polymer chains,[23] the resultant structure of the adsorbed LLDPE layer formed in Wang and co-workers' work may be quite different from that found in the present study. This may cause different substrate effects on the recrystallized structures for very thin (a few tens of nanometers or less in thickness) semicrystalline polymer films. Further studies are in progress to clarify this point.

V. CONCLUSIONS

By using *in situ* GISAXS and GID techniques, we have investigated the recrystallized structures of LLDPE films with the three different thicknesses (25, 50, and 100 nm) prepared on clean hydrogen-passivated silicon substrates. In order to elucidate the heterogeneity of the recrystallized structures in the direction normal to the surface, the two modes (the surface-mode and film-mode) with the different incident angles of X-ray beams were used for both GID and GISAXS. The GID results have revealed the presence of the edge-on lamellae at the surfaces and in the interior of the LLDPE films as thin as 25 nm in thickness. We also found that the degree of the crystallinity for the 25 nm thick film is almost half of those for the 50 and 100 nm thick films. The GISAXS results support that the melting process in the interior of the LLDPE films as thin as 25 nm in thickness is governed by the sequential melting as seen in the bulk.[28−30] At the same time, the GISAXS results indicate the presence of the substrate-bound edge-on lamellar layer which persists at least up to T = 150 °C ≫ T_m (=117 °C), regardless of the film thickness. Intensive washing of the films with toluene uncovered the presence of the very thin (about 10 nm in thickness) residual edge-on lamellar layer, which is likely the origin of the substrate-bound lamellar layer. Moreover, the GISAXS results indicate the loss of the long periods at the topmost surface of the 25 nm thick film at $T \ll T_m$, while the intermediate region (i.e., the transition zone) between the topmost surface and substrate-bound lamellar layer shows the well-ordered lamellar structures. These heterogeneous structures can be explained as a consequence of the nucleation initiated from the substrate-bound lamellar surface, independently of the primary nucleation at the polymer/air interface.[19] The systematic GID and GISAXS results have clarified that the heterogeneous structures induced by the substrate-bound lamellar layer exist within the region of 50 nm in thickness from the substrate interface. Since the formation of both the adsorbed layer and the transition zone near the substrate interface occurs irrespective of polymer/substrate interactions and flexibility of polymer chains,[9,22−27] the heterogeneous structures discovered in the present study (i.e., for the weakly interacting system) would be likely general and hence crucial for manipulating the properties of ultrathin semicrystalline polymer films.

AUTHOR INFORMATION

Corresponding Author

*E-mail: tkoga@notes.cc.sunysb.edu (T.K.); mkoga@notes.cc.sunysb.edu (M.K.E.); takahara@cstf.kyushu-u.ac.jp (A.T.).

Notes

The authors declare no competing financial interest.

ACKNOWLEDGMENTS

We acknowledge ExxonMobil Corporation for providing the LLDPE resin. T.K. acknowledges the financial support from NSF Grant No. CMMI-084626 and Kuraray Co., Ltd., Japan. P.G. acknowledges the financial support from the NSF East Asia and Pacific Summer Institutes Program and the Summer Fellowship from The Japan Society for the Promotion of Science. D.S. and M. L. acknowledge the support from the NSF/DOE under grant number NSF/CHE-0822838. Uses of the Advanced Photon Source and the National Synchrotron Light Source were supported by the U.S. Department of Energy, Office of Science, Office of Basic Energy Sciences, under Contracts No. DE-AC02-06CH11357 and No. DE-AC02-98CH10886, respectively. The GISAXS measurements for the adsorbed layer were carried out at the BL03XU frontier soft-material beamline (FSBL, SPring-8, Japan) with the proposal No. 2011B7256.

REFERENCES

(1) Hamley, I. W. *Prog. Polym. Sci.* **2009**, *34*, 1161.
(2) Hu, H. W.; Granick, S. *Science* **1992**, *258*, 1339.
(3) Bodiguel, H.; Fretigny, C. *Phys. Rev. Lett.* **2006**, *97*, 266105.
(4) Ellison, C. J.; Torkelson, J. M. *Nat. Mater.* **2003**, *2*, 695.
(5) Fakhraai, Z.; Forrest, J. A. *Phys. Rev. Lett.* **2005**, *95*, 025701.
(6) Zheng, X.; Rafailovich, M. H.; Sokolov, J.; Strzhemechny, Y.; Schwarz, S. A.; Sauer, B., B.; Rubinstein, M. *Phys. Rev. Lett.* **1997**, *79*, 241.
(7) Li, C.; Kim, H.; Jiang, J.; Li, C.; Koga, T.; Lurio, L. B.; Schwarz, S.; Narayanan, S.; Lee, H.; Lee, Y.-J.; Jiang, J.; Sinha, S. K.; Rafailovich, M. H.; Sokolov, J. C. *Europhys. Lett.* **2006**, *73*, 899.
(8) Priestley, R. D.; Ellison, C.; Broadbelt, L. J.; Torkelson, J. M. *Science* **2005**, *309*, 456.
(9) Koga, T.; Jiang, N.; Gin, P.; Endoh, M. K.; Narayanan, S.; Lurio, L. B.; Sinha, S. K. *Phys. Rev. Lett.* **2011**, *107*, 225901.
(10) Fakhraai, Z.; Forrest, J. A. *Science* **2008**, *319*, 600.
(11) Yang, Z.; Fujii, Y.; Lee, F. K.; Lam, C.-H.; Tsui, O. *Science* **2010**, *328*, 1676.
(12) Koga, T.; Li, C.; Endoh, M.; Koo, J.; Rafailovich, M. H.; Narayanan, S.; Lee, D. R.; Lurio, L.; Sinha, S. K. *Phys. Rev. Lett.* **2010**, *104*, 066101.
(13) Frank, C. W.; Despotopoulou, M. M.; Pease, R. F. W.; Hinsberg, W. D.; Miller, R. D.; Rabolt, J. F. *Science* **1996**, *273*, 912.
(14) Reiter, G.; Sommer, J. U. *J. Chem. Phys.* **2000**, *112*, 4376.
(15) Cho, K.; Kim, D.; Yoon, S. *Macromolecules* **2003**, *36*, 7652.
(16) Schönherr, H.; Frank, C. W. *Macromolecules* **2003**, *36*, 1199.
(17) Wang, Y.; Ge, S.; Rafailovich, M.; Sokolov, J.; Zou, Y.; Ade, H.; ning, J. L.; Lustiger, A.; Maron, G. *Macromolecules* **2004**, *37*, 3319.
(18) Wang, Y.; Rafailovich, M.; Sokolov, J.; Gersappe, D.; Araki, T.; Zou, Y.; Kilcoyne, A. D. L.; Ade, H.; Marom, G.; Lustiger, A. *Phys. Rev. Lett.* **2006**, *96*, 028303.

(19) Wang, Y.; Chan, C.-M.; Ng, K.-M.; Li, L. *Macromolecules* **2008**, *41*, 2548.
(20) Yakabe, H.; Sasaki, S.; Sakata, O.; Takahara, A.; Kajiyama, T. *Macromolecules* **2003**, *36*, 5905.
(21) Jukes, P. C.; Das, A.; Durell, M.; Trolley, D.; Higgins, A. M.; Geoghegan, M.; Macdonald, J. E.; Jones, R. A. L.; Brown, S.; Thompson, P. *Macromolecules* **2005**, *38*, 2315.
(22) Napolitano, S.; Pilleri, A.; Rolla, P.; Wubbenhorst, M. *ACS Nano.* **2010**, *4*, 841.
(23) Napolitano, S.; Wübbenhorst, M. *Nature Commun.* **2011**, *2*, 260.
(24) Napolitano, S.; Wübbenhorst, M. *J. Phys. Chem. B* **2007**, *111*, 9197.
(25) Napolitano, S.; Prevosto, D.; Lucchesi, M.; Pingue, P.; D'Acunto, M.; Rolla, P. *Langmuir* **2007**, *23*, 2103.
(26) Lan, Q.; Yu, J.; Zhang, J.; He, J. *Macromolecules* **2011**, *44*, 5743.
(27) Fujii, Y.; Yang, Z. H.; Leach, J.; Atarashi, H.; Tanaka, K.; Tsui, O. K. C. *Macromolecules* **2009**, *42*, 7418.
(28) Belbeoch, B.; Guinier, A. *Makromol. Chem.* **1959**, *31*, 1.
(29) Crist, B. *Macromolecules* **2003**, *36*, 4880.
(30) Crist, B. *J. Polym. Sci. B: Polym. Phys.* **2001**, *39*, 2454.
(31) Wu, S. *J. Macromol. Sci. Part C* **1974**, *10*, 1.
(32) Kwok, D. Y.; Neumann, A. W. *Adv. Colloid Interac.* **1999**, *81*, 167.
(33) Hamada, F.; Wunderlich, B.; Sumida, T.; Hayashi, S.; Nakajima, A. *J. Phys. Chem.* **1968**, *72*, 178.
(34) Khanna, V.; Cochran, E. W.; Hexemer, A.; Stein, G. E.; Fredrickson, G. H.; Kramer, E. J.; Li, X.; Wang, J.; Hahn, S. F. *Macromolecules* **2006**, *39*, 9346.
(35) Wu, W. L.; Wallace, W. E.; van Zanten, J. H.; Bauer, B. J.; Liu, D. W.; Wong, A. *Polymer* **1997**, *38*, 2583.
(36) Tashiro, K.; Ishino, K.; Ohta, T. *Polymer* **1999**, *40*, 3469.
(37) Chen, X.; Christian, C.; Ruan, D.; Zhang, L.; Hsiao, B. S.; Chu, B. *Polymer* **2006**, *47*, 2839.
(38) Vonk, C. G.; Kortleve, G. *Kolloid-Z. Z. Polym.* **1967**, *220*, 19.
(39) Slusarczyk, C. *J. Alloys Compd.* **2004**, *382*, 68.
(40) Debye, P.; Bueche, A. M. *J. Appl. Phys.* **1949**, *20*, 518.
(41) Ruland, W. *J. Pppl. Cryst.* **1971**, *4*, 70.
(42) Nam, J. Y.; Kadomatsu, S.; Saito, H.; Inoue, T. *Polymer* **2002**, *43*, 2101.
(43) Albrecht, T.; Strobl, G. *Macromolecules* **1995**, *28*, 5827.
(44) Wunderlich, B., *Macromolecular Physics*; Academic Press: New York, 1973.
(45) Mandelkern, L., *Crystallization of Polymers*; McGraw-Hill: New York, 1984.
(46) Masunaga, H.; Ogawa, H.; Takano, T.; Sasaki, S.; Goto, S.; Tanaka, T.; Seike, T.; Takahashi, S.; Takeshita, K.; Nariyama, N.; Ohashi, H.; Ohata, T.; Furukawa, Y.; Matsushita, T.; Ishizawa, Y.; Yagi, N.; Takata, M.; Kitamura, H.; Sakurai, K.; Tashiro, K.; Takahara, A.; Amamiya, Y.; Horie, K.; Takenaka, M.; Kanaya, T.; Jinnai, H.; Okuda, H.; Akiba, I.; Takahashi, I.; Yamamoto, K.; Hikosaka, M.; Sakurai, S.; Shinohara, Y.; Okada, A.; Sugihara, Y. *Polym. J.* **2011**, *43*, 471.
(47) Yang, J. P.; Liao, Q.; Zhou, J. J.; Jiang, X.; Wang, X. H.; Zhang, Y.; Jiang, S. D.; Yan, S. K.; Li, L. *Macromolecules* **2011**, *44*, 3511.
(48) Thomas, K. R.; Chenneviere, A.; Reiter, G.; Steiner, U. *Phys. Rev. E* **2011**, *83*, 021804.
(49) Barbero, D. R.; Steiner, U. *Phys. Rev. Lett.* **2009**, *102*, 248303.
(50) Metin, B.; Blum, F. D. *J. Chem. Phys.* **2006**, *125*, 054707.
(51) Wallace, W. E.; van Zanten, J. H.; Wu, W. L. *Phys. Rev. E* **1995**, *52*, R3329.
(52) van Zanten, J. H.; Wallace, W. E.; Wu, W. L. *Phys. Rev. E* **1996**, *53*, R2053.
(53) Zhang, F.; Baralia, G. G.; Nysten, B.; Jonas, A. M. *Macromolecules* **2011**, *44*, 7752.
(54) Reiter, G. *J. Polym. Sci., Part B: Polym. Phys.* **2003**, *41*, 1869.
(55) Sommer, J.-U.; Reiter, G. *Europhys. Lett.* **2001**, *56*, 755.